ceramics

MDPI

Article

Sinterability, Mechanical Properties and Wear Behavior of Ti_3SiC_2 and Cr_2AlC MAX Phases

Eduardo Tabares [1], Michael Kitzmantel [2], Erich Neubauer [2], Antonia Jimenez-Morales [1] and Sophia A. Tsipas [1,*]

[1] Departamento de Ciencia e Ingeniería de Materiales e Ingeniería Química, IAAB, Universidad Carlos lll de Madrid, Avda. De la Universidad 30, 38911 Leganés, Spain; etabares@ing.uc3m.es (E.T.); toni@ing.uc3m.es (A.J.-M.)

[2] RHP-Technology GmbH, Forschungs- und Technologiezentrum, 2444 Seibersdorf, Austria; m.ki@rhp.at (M.K.); e.ne@rhp.at (E.N.)

* Correspondence: stsipas@ing.uc3m.es

Abstract: MAX phases are a promising family of materials for several demanding, high-temperature applications and severe conditions. Their combination of metallic and ceramic properties makes MAX phases great candidates to be applied in energy production processes, such as high temperature heat exchangers for catalytic devices. For their successful application, however, the effect of the processing method on properties such as wear and mechanical behavior needs to be further established. In this work, the mechanical and wear properties of self-synthesized Ti_3SiC_2 and Cr_2AlC MAX phase powders consolidated by different powder metallurgy routes are evaluated. Uniaxial pressing and sintering, cold isostatic pressing and sintering and hot pressing were explored as processing routes, and samples were characterized by analyzing microstructure, phase constitution and porosity. Wear behavior was studied by reciprocating-sliding tests, evaluating the wear rate by the loss of material and the wear mechanism.

Keywords: Ti_3SiC_2; Cr_2AlC; MAX phases; reciprocating-sliding; wear behavior; mechanical properties; hot isostatic pressing; powder processing

Citation: Tabares, E.; Kitzmantel, M.; Neubauer, E.; Jimenez-Morales, A.; Tsipas, S.A. Sinterability, Mechanical Properties and Wear Behavior of Ti_3SiC_2 and Cr_2AlC MAX Phases. *Ceramics* **2022**, *5*, 55–74. https://doi.org/10.3390/ceramics5010006

Academic Editors: Margarita A. Torresani and Elisa Torresani

Received: 14 December 2021
Accepted: 29 January 2022
Published: 31 January 2022

1. Introduction

Nanolaminated ternary carbides and nitrides, MAX Phases, are a new family of materials with great potential for different highly demanding and aggressive environments [1,2]. Due to their structure, MAX phases show good mechanical properties at high temperatures [3] with good oxidation and corrosion behaviors, and at the same time, exhibit good electrical and thermal conductivity and are easily machinable [4,5]. MAX phases' name comes from the elements that configure the ternary compound: M is an early transition metal, A is an element of the groups IIIA and IVA of the periodic table and X is either carbon or nitrogen. They exhibit a fixed stoichiometry and a general formula of $M_{n+1}AX_n$, where n is a number between 1 and 3 [4,6]. This excellent combination of ceramic and metallic-like properties occurs as a result of the layered disposition of the elements in the structure, alternating layers of elements MX and layers of element A, making this family of materials a good candidate for several applications [3]. In recent years, there has been a search for different applications for the use of this family of materials. Their use as heat exchangers [7] or catalytic devices using porous Ti_3SiC_2 and Ti_2AlC [8], thermal barriers using Cr_2AlC [9] or as fuel cladding material in nuclear reactors using Zr_2AlC [10] are some of the possible applications of these materials.

As for the wear behavior of MAX phases, several works have characterized the resistance of this family of materials under abrasive conditions. El-Raghy et al. [11] studied the effect of the grain size on the wear behavior of hot-isostatically-pressed (HIP) Ti_3SiC_2 samples by pin-on-disk tests and found a large difference in the coefficient of friction (COF)

at initial stages and a similar final COF once the debris started acting as a third body. Magnus et al. [12] explored the wear mechanism of a dual Ti_3AlC_2-Ti_2AlC MAX phase and the evolution of the microstructure by the pin-on-disk test, proposing a three-body abrasive wear with a wear rate of 10^{-4} mm^3/Nm. Shamsipoor et al. [13] analyzed the effect of the spark plasma sintering (SPS) parameters on the wear behavior of Cr_2AlC. Although the SPS parameters mainly affected the final MAX phase composition, which was synthesized in situ from elemental powders, wear behavior improved with the presence of the Cr_2AlC phase, with mainly adhesion and delamination wear mechanisms. In addition to this, MAX phases have been studied as a reinforcement for other materials in order to improve wear behavior. Yu et al. [14] produced an AZ91 magnesium composite reinforced with the Ti_2AlC MAX phase, improving the wear resistance in pin-on-disk wear tests with the addition of a MAX phase when compared to the raw magnesium alloy. From these works, it can be observed that the wear behavior of MAX phases is commonly studied in samples that are synthesized during the consolidation process and not starting from raw MAX phases powders, as it is in the scope of this work.

One of the main issues of pin-on-disk tests is the control of the constant load when starting the test; generally, the surface is smooth, but as time passes, wear products build up, causing the bolt that contains the counter material to vibrate. Although reciprocating-sliding tests do not maintain a constant velocity during the test, they offer a study of the reciprocal slip generated in the samples that is interesting for real industry behaviors, mainly in the biomedical industry [15]. Reciprocating-sliding tests are based on the application of a constant normal load over the sample through a bolt enclosing the counter material. This bolt performs a reciprocal movement with a previously defined stroke at the desired frequency. This method has the advantage of producing many repetitions of the sliding cycles, which causes the friction and wear processes to reach a stable value faster than other techniques [16].

As commented before, MAX phases are most frequently synthesized during their consolidation step and characterized after the optimization of the process [17–19]. Nevertheless, this work aims to study the consolidation process of already self-synthesized high purity Ti_3SiC_2 and Cr_2AlC MAX phase powders in order to validate the powder production process and analyze the sinterability of the powder through different consolidation methods: uniaxial pressing and sintering, cold isostatic pressing and sintering and hot pressing. Sintered samples were analyzed in order to determine the relative density of the processed samples, and the mechanical properties and wear behavior of selected samples were studied.

2. Materials and Methods

2.1. Powder Characterization

Self-synthesized and high purity Ti_3SiC_2 and Cr_2AlC MAX phases were produced from the commercially available powders detailed in Table 1, and the powder synthesis was scaled-up for large-quantity powder production. Ti_3SiC_2 was obtained starting from Ti:SiC:C with a molar ratio of 3:1,5:0,5 [20] and Cr_2AlC MAX phase was obtained by the synthesis of the elemental powders of Cr:Al:C with a molar ratio of 2:1,2;1.

Table 1. A list and the characteristics of commercially available powders for the synthesis of Ti_3SiC_2 and Cr_2AlC MAX phases.

Powder	Supplier	D50 (μm)	D90 (μm)	Purity (%)
Ti	TLS Technik GmbH, Bitterfeld-Wolfen, Germany	8	14	99
SiC	Navarro S.A., León, Spain	12	21	99.5
C	Ismaf S.L., Zamudio, Spain	24	58	99.5
Cr	Goodfellow Ltd., Huntingdon, UK	30	53	99.5
Al	AEE, Upper Saddle River, NJ USA	38	79	99.5

After mixing the initial powders in a Turbula shaker mixer (WAB Group, Muttenz, Switzerland) for 1 h, the powders were isostatically cold pressed at 4000 bar (EPSI Systems, Temse, Belgium). The synthesis of the pressed pellets was achieved by pressureless sintering. For the Ti_3SiC_2 MAX phase, a tubular high vacuum furnace was used (2.5×10^{-5}, HVT-15/50/450, Carbolite, Hope, UK) at 1300 °C for 6 h, with heating and cooling rates of 5 °C/min; for the Cr_2AlC MAX phase, a tubular furnace (STF-15/757450, Carbolite, Hope, UK) with an argon atmosphere was used at 1300 °C for 4 h, with heating and cooling rates of 5 °C/min. Synthesized consolidated samples were then crushed in a planetary ball mill (Pulverisette 5/2, Fritsch, Weimar, Germany) using a powder to ball ratio of 10:1, with isopropanol as a mixing medium and an argon protective atmosphere. After drying the synthesized powder in air at 100 °C, a comprehensive characterization was performed to study the purity and properties of the powders. Detected phases were analyzed by X-ray diffraction (XRD, Philips X'pert, Almelo, Netherlands) with Cu Kα radiation at 40 kV and 40 mV. The purity of the powders was determined by a least-squared procedure of the most intense peaks of the diffraction spectrum, as reported elsewhere [17]. This method has been previously compared to a Rietveld analysis [20], obtaining similar results for phase quantification. The calculation was done following Equation (1), where I_x corresponds to the integrated area of the most intense peak of the phase to be quantified and I_t to the sum of the integrated area of the most intense peaks detected in the XRD analysis:

$$\% \, Phase = I_x / I_t, \tag{1}$$

In addition, the morphology of the powders was studied with Scanning Electron Microscopy (SEM, TENEO-FEI, Eindhoven, Netherlands) coupled with energy-dispersive X-ray spectroscopy (EDS, DX-4-EDAX, Mahwah, NJ, USA). Furthermore, the mean particle size distribution of the initial powders was measured by Dynamic Light Scattering (MasterSizer 2000, Malvern Instruments, Malvern, UK).

2.2. Consolidation Techniques and Mechanical Properties Characterization

The sinterability of the powders by conventional powder metallurgy, press and sintering, was analyzed in order to understand the consolidation process of the synthesized MAX phase powders. For this purpose, the powders were uniaxially pressed from 100 to 500 MPa and sintered at 1300 °C for 6 h. The Archimedes density was measured for both green and sintered samples to study the effect of the pressure on the densification of the samples.

Alternative powder processing routes were explored. First, instead of uniaxial pressing, powders were cold isostatically pressed (CIP) at 4000 bar and then sintered under the same conditions. Second, inductive hot pressing was optimized to consolidate the MAX phase powders. The influences of pressure, time and temperature on the density of the MAX phase samples were analyzed. For the inductive hot-pressed samples, a 20 mm graphite die was used. The die was covered with a graphite foil with a sprayed coating of boron nitride to reduce the possible reaction of the powders with the die and to facilitate the sample release after the process. The process was performed using two heating rates. First, the heat was increased at a rate of 50 °C/min up to 100 °C below the selected consolidation temperature, then the rate was lowered to 25 °C/min in order to maintain better control of the process temperature. After the programmed dwell time, a cooling rate of 50 °C/min was applied. All processed samples were characterized by SEM and XRD in order to control MAX phase purity after consolidation. In order to understand the reaction mechanism of the hot-pressed samples, thermodynamic calculations of ΔG were performed using Thermo-Calc software (Stockholm, Sweden) with databases SSOL5 and SSUB5 [21].

Vickers hardness measurements were performed in a Zwick Roell Z 2.5 tester with a force of 10 N. Additionally, Young's modulus and elastic and plastic work were measured using a speed for the load applied of 1 mm/min and a speed of 2 mm/min for load removal during the indentation. In addition, cyclic micro-compressive tests (Microtest, EM2/5/FR, Madrid, Spain) were performed to wire-cut cylindrical samples with a height of 6 mm and a diameter of 3 mm. A preload speed of 0.1 mm/min was selected up to 20 N to ensure the

correct contact between the sample and the clamp. Tests were performed at 1 N/s up to 500 N for 5 cycles at room temperature.

2.3. Wear Tests

For the wear characterization of the selected samples, a reciprocating lineal sliding tribometer was used (UMT, Bruker, Mannheim, Germany). A 5 mm alumina ball was used as the counter material for the test, in air, under unlubricated conditions. All of the tests were performed using a 5 mm stroke distance with a frequency of 1 Hz for 30 min. Applied loads were varied from 5 to 10 N, to study the influence of this parameter on the wear rate. Three wear tests were performed for each condition, and the coefficient of friction (COF) was measured during each test. Specific wear rates (W_v) were calculated using the following Equations (2)–(4) reported by Doni et al. [16] to calculate the volume loss (V) divided by the load applied (N) and the total sliding distance (S):

$$W_V = \Delta V / N \cdot S, \tag{2}$$

The volume loss (V) is calculated using the radius (R) of the ball used as counter material, the average depth of the wear track ($\overline{D}$), the average wear loss area ($\overline{A}_w$) from the 2D profiles of the track and the stroke length (l).

$$\Delta V = \left[(1/3) \cdot \pi \cdot \overline{D}^2 \left(3R - \overline{D}\right)\right] + \overline{A}_w \cdot l, \tag{3}$$

Calculating the average depth ($\overline{D}$), through the average wear loss area ($\overline{A}_w$) and the average width of the track ($\overline{W}$).

$$\overline{D} = \overline{A}_w / \overline{W}, \tag{4}$$

Track measurements for the wear rate calculations were performed in an optical profilometer (DSX500, Opto-Digital Microscope, Tokio, Japan) to evaluate three different profiles in the center, top and bottom parts of the track, averaging the width, depth and area of the profiles.

3. Results and Discussion

3.1. Powders Characterization and Sinterability of Ti_3SiC_2 and Cr_2AlC MAX Phases

MAX phase Ti_3SiC_2 and Cr_2AlC synthesized powders are shown in Figure 1. From the micrographs, the irregular morphology of the powders can be observed. In addition, it is possible to see the characteristic nanolaminated structure of the MAX phases [4]. Complementary to the X-ray diffraction patterns of the powders shown in Figure 2, it is possible to observe the presence of some secondary phases, corresponding to $TiSi_2$ in the case of the production of Ti_3SiC_2, and Cr_5C_3 for Cr_2AlC. From the least-square analysis performed on the XRD diffractograms, a total purity of 92 vol.% and 96 vol.% has been calculated for Ti_3SiC_2 and Cr_2AlC, respectively. No other intermediate phase, unreacted powders or contamination from the milling was found from the XRD and EDS analyses of the synthesized powders. Furthermore, the particle size distribution of the powders produced exhibited a high control of the powders' production, with unimodal distribution for both MAX phases and a relatively low mean particle size, obtaining a D_{90} of 20 μm for Ti_3SiC_2 and 23 μm for Cr_2AlC.

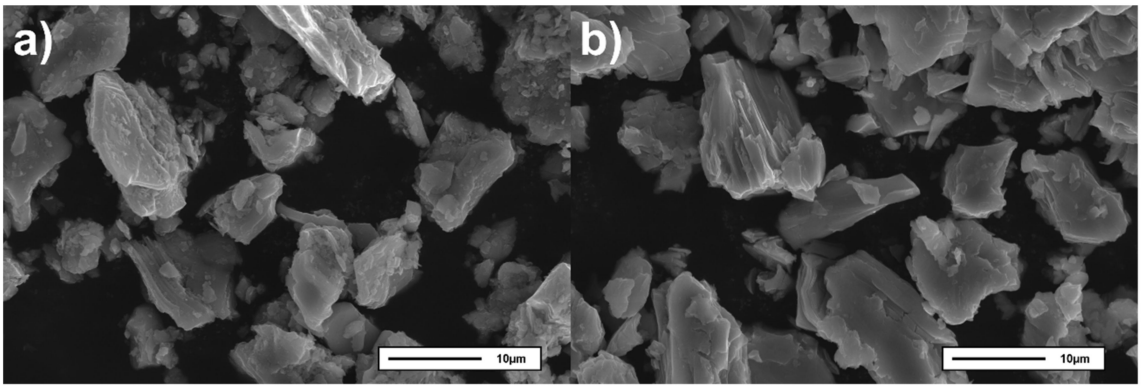

Figure 1. SEM micrographs of self-synthesized powders of (**a**) Ti3SiC2 and (**b**) Cr2AlC MAX phases.

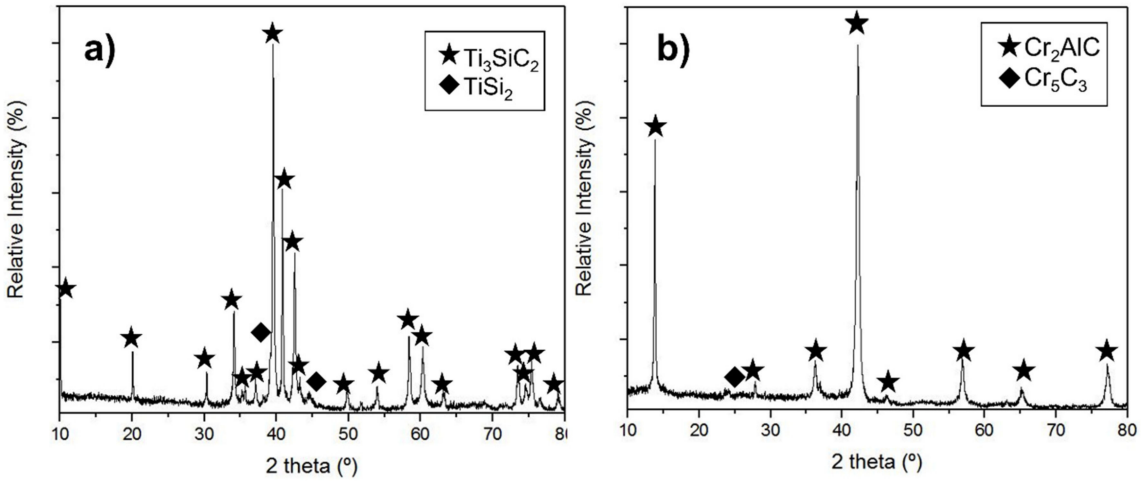

Figure 2. The X-Ray diffraction patterns of self-synthesized powders of (**a**) Ti_3SiC_2 and (**b**) Cr_2AlC MAX phases.

The sinterability properties of both self-synthesized MAX phase powders through conventional powder metallurgy processes were analyzed in order to study the densification of the powders for comparison with other production methods. It is important to note that compressibility tests of the powders through press and sintering establish a starting point to improve the densification or tailor the porosity of the samples, depending on the application. In Figure 3a, the evolution of the relative green density of the samples related to the pressure applied during the consolidation can be observed. A typical behavior is observed, wherein the green density increases with the increase of pressure for both MAX phases. A similar green relative density is exhibited for these samples with up to 63% for Ti_3SiC_2 and 61% for Cr_2AlC at 500 MPa. Both MAX phases show a similar slope while increasing the pressure. In addition, the evolution of the volumetric relative density after sintering was calculated (Figure 3b). It is possible to observe an increase in the relative density of the samples with the increase of the pressure up to 400 MPa and a stabilization of the value after this value, obtaining a relative density of 75% and 88% for Ti_3SiC_2 and Cr_2AlC, respectively, after sintering. Although the green density slopes showed a similar behavior in the green state, it is possible to observe a difference in the final relative density of the sintered samples. Generally, the hardness values of the materials have a direct correlation with the compressibility properties of the powders. From the theoretical values of Ti_3SiC_2 (4 GPa) [22] and Cr_2AlC (5.5 GPa) [23], it can be seen how this effect is not correlated. The lower compressibility of the powders appears to be an effect of the different particle size distribution of the powders, obtaining a lower compressibility for Ti3SiC2 (D_{90} = 20 µm) than for Cr_2AlC (D_{90} = 23 µm). These relative density values, albeit

low, might prove beneficial for applications such as catalytic substrates [24] electrodes [25], volumetric solar receivers [26] or hot gas filters [27].

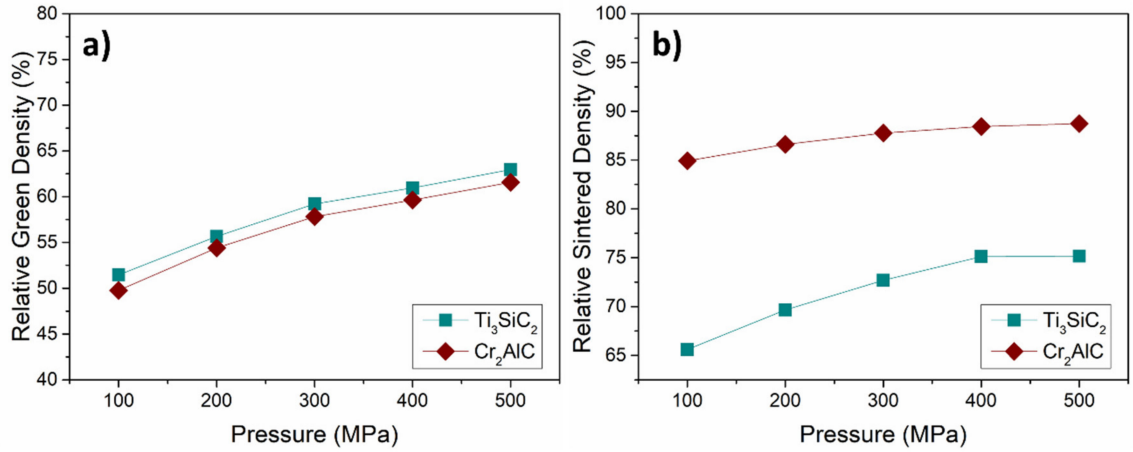

Figure 3. The press and sintering density measurements of Ti_3SiC_2 and Cr_2AlC: (**a**) relative green density and (**b**) relative sintered density.

The optimization of the hot-pressing process was done by analyzing the possible decomposition of the MAX phases after the process. First, the Ti_3SiC_2 MAX phase was hot pressed at a range of temperatures using a fixed pressure (30 MPa) and holding time of 15 min. XRD analysis of the samples after the process showed the limiting temperatures to avoid decomposition of the Ti_3SiC_2 phase. As can be observed in Figure 4, at a low temperature of 1050 °C, the phases present in the final samples correspond to Ti_3SiC_2 and the intermediate phase $TiSi_2$, which is also present in the initial composition of the powders. As the temperature begins to increase, the formation of TiC begins, reaching a maximum in its formation at 1250 °C, along with the decomposition of the MAX phase. This effect can be better seen in Figure 4b, where the amount of TiC at 1150 °C is 8%, increasing to 85% at 1250 °C. The phase formation of TiC could be due to the reactions produced by different effects, as discussed below. First, inductive heating, combined with pressure, accelerates the reactions that occur inside the graphite mold, altering the reactions studied in the pressureless sintering processes [20]. In addition to this, although a B/N sprayed coating is applied, it is possible that the powders react with the graphite foil; this could enhance the formation of TiC by reacting with the impurities of $TiSi_2$. These effects are correlated with the Gibbs free energy calculations of the possible reactions occurring during the hot pressing process, as shown in Table 2. Reaction 1 corroborates the stability of the MAX phase Ti_3SiC_2, which should not decompose at these temperatures, although from experimental synthesis of this MAX phase, it was observed that decomposition is possible at temperatures above 1300 °C [20]. TiC presence at temperatures of 1050 °C is in accordance with reaction 2, where the existence of the intermediate phase $TiSi_2$ and C produces TiC and $Si_{(gas)}$. Comparing the Gibbs free energy values from 1050 °C to 1350 °C to those presented elsewhere [20], it is possible to observe that the formation of TiC is more thermodynamically stable than the formation of Ti_3SiC_2, enhancing the appearance of TiC while the decomposition of Ti_3SiC_2 is occurring. Argon was used during the hot-pressing of the Ti_3SiC_2 to study the possible influence of using a protective atmosphere during the process; nevertheless, this effect could not be controlled, obtaining the same decomposition products in the final samples. With all this in mind, a temperature of 1150 °C was selected as optimal for the consolidation of Ti_3SiC_2 by inductive hot pressing. In addition to the temperature analysis, pressure and holding time at maximum temperature were varied to study the final density of the consolidated sample. By increasing the pressure on the sample to 50 MPa, it was possible to improve the density by 5%, reaching a total of 74% relative density, and by increasing the holding time to 1 h, up to an 80% densification was reached. On the other hand, for Cr_2AlC,

from the XRD analysis in Figure 5, there is no decomposition or increase in the secondary phase formation during the consolidation of the powders for all tested temperatures, and a temperature of 1200 °C was selected for this process.

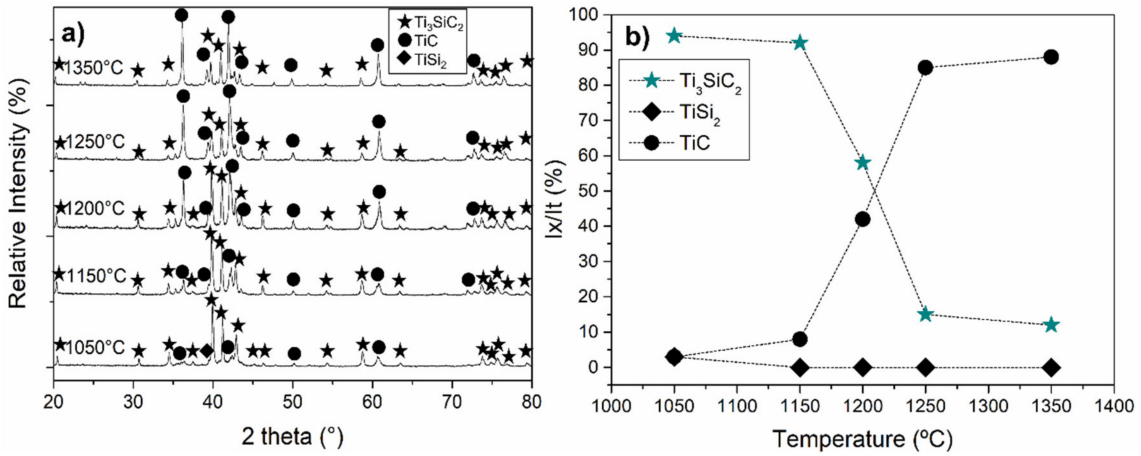

Figure 4. (**a**) The X-ray diffraction patterns of hot-pressed Ti_3SiC_2 powders from 1050 °C to 1350 °C and (**b**) the phase evolution from the XRD profiles.

Table 2. The Gibbs free energy calculations of different possible reactions during the hot pressing process at temperatures ranging from 1050 °C to 1350 °C.

Reaction	ΔG [J] 1050 °C	1150 °C	1200 °C	1250 °C	1350 °C
$Ti_3SiC_2 + C \rightarrow 3TiC + Si(g)$	4.47×10^3	2.83×10^4	4.06×10^4	5.31×10^4	7.87×10^4
$TiSi_2 + C \rightarrow TiC + 2Si(g)$	-4.80×10^5	-4.47×10^5	-4.31×10^5	-4.13×10^5	-3.79×10^5

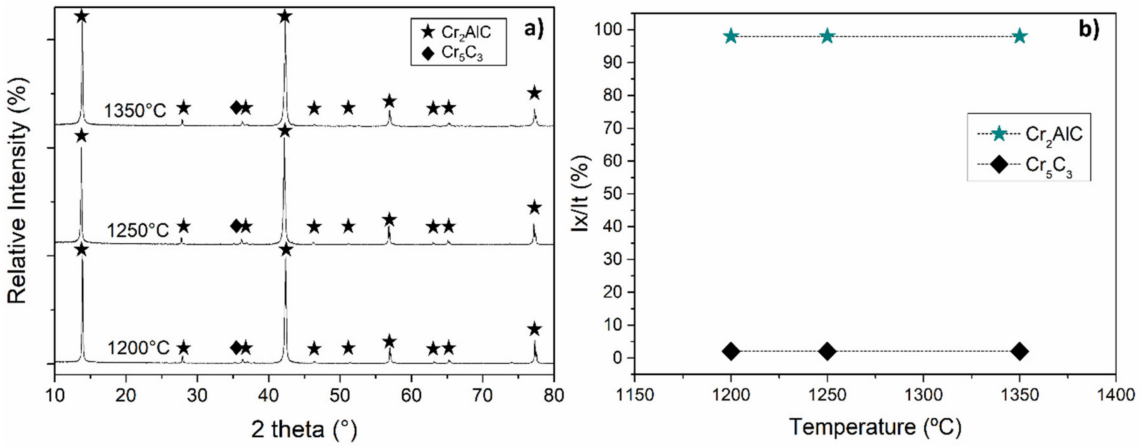

Figure 5. (**a**) The X-ray diffraction patterns of hot-pressed Cr_2AlC powders from 1200 °C to 1350 °C and (**b**) the phase evolution from the XRD profiles.

A summary of the microstructures obtained for the three different processes is shown in Figure 6, and the relative densities of each process are shown in Table 3. Isostatic pressing improves the densification of the samples when compared to press and sintering, and hot pressing enhances the densification of the Cr_2AlC MAX phase even further. For Ti_3SiC_2, density doesn't improve with the hot pressing process; the lower particle size distribution of this powder, combined with the reaction of the powder with the die and decomposition during the process, may have a negative effect on the consolidation of this MAX phase. From the XRD analysis of the consolidated samples shown in Figure 7, the high purity of

the processed samples is corroborated. For pressed and sintered samples (uniaxially and cold isostatically), it is possible to see remnants of secondary $TiSi_2$ from the initial powder synthesis for Ti_3SiC_2 (Figure 7a) and the minor presence of Cr_5C_3 in the Cr_2AlC (Figure 7b) consolidated samples. For hot-pressed samples, no decomposition of Ti_3SiC_2 was found after the consolidation process, with only TiC as a secondary phase (Figure 7a). In the case of Cr_2AlC, the XRD analysis (Figure 7b) shows a minor presence of Cr_5C_3 as secondary phase. In addition, the relative densities of the processed samples are shown in Table 3 to study the influence of the processes on the MAX phase samples. Densification of the powders was enhanced by this process obtaining up to 80% of relative density for Ti_3SiC_2 and 95% for Cr_2AlC.

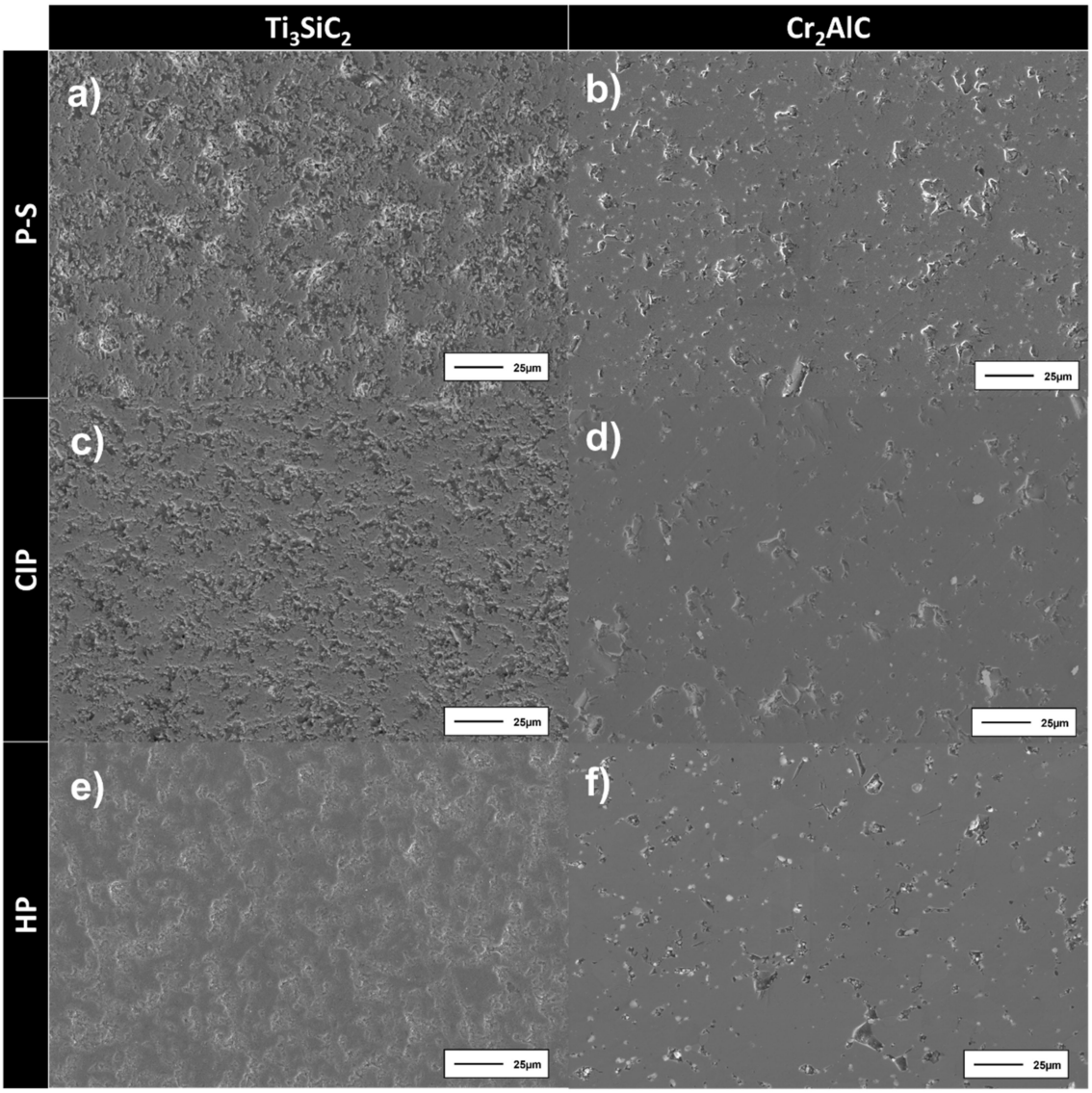

Figure 6. SEM micrographs of consolidated samples by different routes: (**a**) uniaxially pressed and sintered (P-S) Ti_3SiC_2; (**b**) uniaxially pressed and sintered (P-S) Cr_2AlC; (**c**) cold isostatic pressed and sintered (CIP) Ti_3SiC_2; (**d**) cold isostatic pressed and sintered (CIP) Cr_2AlC; (**e**) hot-pressed (HP) Ti_3SiC_2 and (**f**) hot-pressed (HP) Cr_2AlC.

Table 3. The relative densities of the consolidated Ti_3SiC_2 and Cr_2AlC MAX phases by press and sintering (P-S), cold isostatic pressing and sintering (CIP) and hot-pressing (HP).

Material	Process	Relative Density (%)
Ti_3SiC_2	P-S	75
	CIP	83
	HP	80
Cr_2AlC	P-S	88
	CIP	95
	HP	96

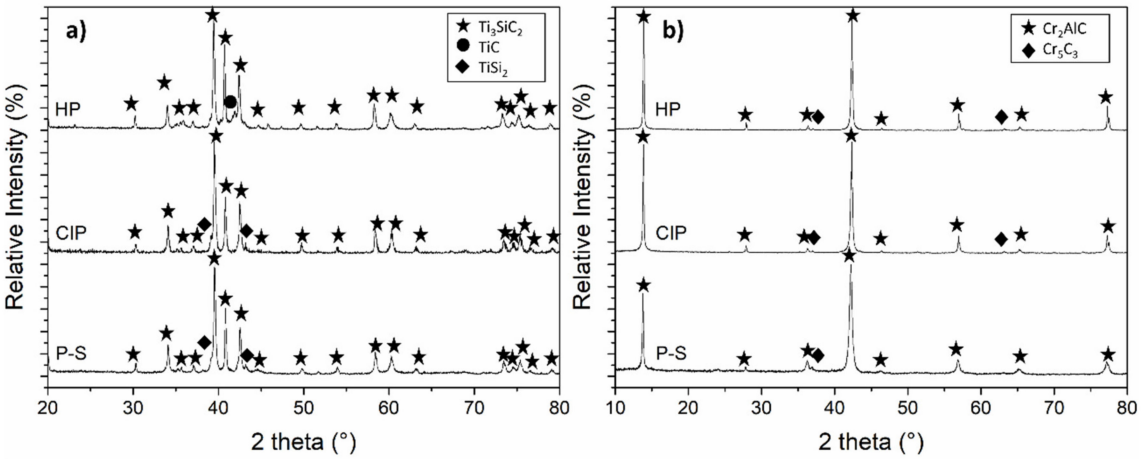

Figure 7. The X-ray diffraction patterns of uniaxially pressed and sintered (P-S), cold isostatic pressed and sintered (CIP) and hot-pressed (HP) consolidated samples after optimization of the process for (**a**) Ti_3SiC_2 at 1150 °C for 1 h and (**b**) Cr_2AlC at 1200 °C for 15 min.

3.2. Effect of the Consolidation Technique on the Mechanical Properties

The hardness, Youngs modulus, elastic and plastic work and recovery indexes calculated for the three processing routes used to consolidate Ti_3SiC_2 and Cr_2AlC are shown in Table 4. From the hardness values, it is possible to see an increase of the value for Ti_3SiC_2 as the consolidation technique is improved, from 136 HV for the P-S sample to 322 HV for the hot-pressed material. Although this value it is not directly correlated to the porosities obtained for each process, the amount of porosity in the samples increases the standard deviation of the measurements. Hardness is mainly dependent on the grain size generated in each process, with hot-pressed samples having a smaller grain size due to their fast consolidation. The same occurs for Cr_2AlC, where hot-pressed samples have a higher hardness value (535 HV) than the P-S (427 HV) and CIP (398 HV), due to the smaller grain size. Hardness values reported for Ti_3SiC_2 obtained through in situ synthesis reach values around 600 HV [5], which are higher than those obtained in this work (322 HV). In the case of Cr_2AlC, hardness values obtained for the hot-pressed samples (535 HV) are similar to those previously reported (530 HV) [5]. From the elastic and plastic work of the samples, it is important to note a higher value for the plastic work, a behavior that is characteristic of ceramic materials. This plastic work value is higher for the Ti_3SiC_2 MAX phase, and this should have an effect on the wear mechanism of this material, favoring a lower wear resistance and lowering the coefficient of friction as compared to Cr_2AlC for the same porosity values. In terms of the recovery index of the samples, similar values for P-S and CIP samples can be observed, although there is a clear difference in porosity between these samples and the hot-pressed samples; the appearance of localized porosity could have a big effect in this matter, reducing the elastic recovery of the surface after the test. In addition, the smaller grain size of the hot-pressed Ti_3SiC_2 appears to have an influence on the recovery properties of this material. Cr_2AlC recovery indexes are similar

for all the consolidation processes. All consolidated Cr_2AlC samples showed a high relative density and hence the effect of porosity in this recovery value is not significant. In terms of elastic modulus, this value has a great dependence on both the porosity in the sample and the grain size of the material. It can be observed in Figure 8 that lower E modulus values are obtained compared to those previously reported (343 kN/mm^2 for Ti_3SiC_2 and 245 kN/mm^2 for Cr_2AlC) [5]. As the porosity changes depending on the consolidation method in Ti_3SiC_2, and it is lower for cold isostatic pressing and higher for consolidation by hot pressing, the elastic modulus varies in this same manner. In the case of Cr_2AlC, the influence of the grain size directly relates to the higher E modulus obtained for the hot-pressed samples. A decrease in the elastic modulus for the CIP samples can also be observed; this in in accordance with the hardness values obtained and could be due to localized porosity in the sample.

Table 4. A summary of the measured mechanical properties of uniaxially (P-S), cold isostatic pressed and sintering (CIP) and hot-pressed (HP) Ti_3SiC_2 and Cr_2AlC MAX phases. W_{elast} and W_{plast} stand for the elastic and plastic work during the indentation and μ_{IT} for the recovery index after releasing the indentation.

Material	Zone	Hardness (HV10)	W_{elast} (Nmm)	W_{plast} (Nmm)	μ_{IT} (%)
Ti_3SiC_2	P-S	136	0.008 ± 0.001	0.055 ± 0.001	12.5 ± 0.6
	CIP	139	0.008 ± 0.001	0.054 ± 0.002	12.2 ± 0.8
	HP	322	0.021 ± 0.004	0.040 ± 0.004	34.2 ± 4.5
Cr_2AlC	P-S	427	0.008 ± 0.001	0.027 ± 0.002	22.3 ± 1.5
	CIP	398	0.008 ± 0.002	0.029 ± 0.002	22.3 ± 4.0
	HP	535	0.017 ± 0.001	0.024 ± 0.001	24.7 ± 2.5

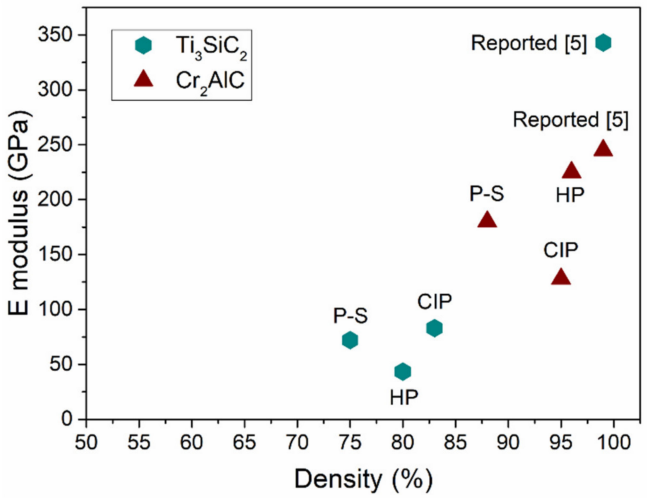

Figure 8. The E modulus of uniaxially (P-S), cold isostatic pressed and sintering (CIP) and hot- pressed (HP) Ti_3SiC_2 and Cr_2AlC MAX phases compared with the reported values from Barsoum, M. 2013.

The cyclic micro-compressive behaviors of cold isostatic pressed and sintered and hot-pressed samples are shown in Figure 9. It is possible to observe for both materials a kinking non-linear elastic behavior characteristic of MAX phases. The twisting that is generated by the energy dissipation during the compression is produced by the formation of incipient kinking bands (IKB) dislocations [4]. It is also possible to observe the lack of hysteresis during the different cycles, since it is not possible to differentiate the load and unload for any of the material. At loads under a specific threshold, IKB dislocations contract, producing a reversible process, thus generating the same values for every cycle and an elastic behavior due to the absence of plastic deformation at this load (500 N). This

effect produces a fully reversible loop for the uniaxial compression of MAX phases, as previous works have shown, for dense and porous MAX phases [28,29].

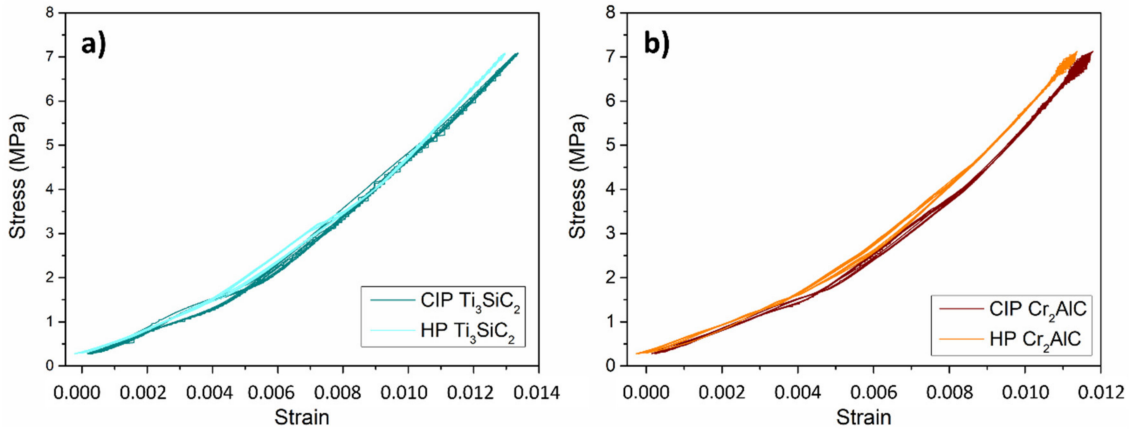

Figure 9. The cyclic micro-compressive stress-strain behavior of CIP and sintered and HP samples of (**a**) Ti_3SiC_2 and (**b**) Cr_2AlC at a load of 500 N with a pressure rate of 1 N/s.

In Figure 9a,b, it is also possible to observe a slight difference between the cold isostatic pressed and sintered and the hot-pressed samples. Although there is a porosity difference between the different sample production routes, this disparity should not be the main factor in the differences of compressive behavior. The main reason for the slight change in rigidity values during the micro-compressive test is the grain size generated during the sample production. This has a strong dependence on the cyclic compressive behavior of MAX phases [3], resulting in a lower strain on the material.

3.3. Effect of the Consolidation Technique on the Wear Behavior of Ti_3SiC_2 and Cr_2AlC MAX Phases and Influence of the Test Load on the Wear Properties

Initially, in order to assess the influence of the grain size on the wear behavior of the samples according to the processing route, a qualitative evaluation of the grain sizes was performed by micrographic analysis, as shown in Figure 10. It is possible to observe the presence of porosity at the grain boundaries of the MAX phases in all of the micrographs. The Ti_3SiC_2 samples exhibit smaller grains, shown in Figure 10a,c (~8 μm for CIP and ~4.5 μm for HP), compared to the Cr_2AlC samples (~32 μm for CIP and ~18 μm for HP) shown in Figure 10b,d. When comparing the different processing routes, it is possible to observe a common trend: Hot-pressed samples exhibit a smaller grain size when compared to the samples processed by cold isostatic pressing and sintering. This could be an effect of the cooling rate of the processes, with lower grain sizes for higher cooling rates.

The evolution of the friction coefficients (COF) during the wear tests is shown in Figure 11 for the Ti_3SiC_2 samples and Figure 12 for the Cr_2AlC samples. It is possible to observe different behaviors for different Ti_3SiC_2 samples (Figure 11). The CIP Ti_3SiC_2 sample tested with a load of 5 N shows a steady increase in the friction coefficient that stabilizes at around 300 s at a COF of 0.65. By increasing the load on the CIP Ti_3SiC_2 sample, it is possible to observe a higher initial coefficient, probably due to the initial debris generated in the track, and after less than a minute, the delamination of this generated debris reduces the abrasive effect, acting as a lubricant and lowering the coefficient value, stabilizing at values close to those of the sample tested at 5 N. This self-lubricant effect has been previously reported for both MAX phases and is intrinsic to the layered hexagonal crystalline structure of MAX phases [12], causing a reduction in the friction coefficient. Furthermore, this lubricating effect is also a result of the oxidation of the loose wear material, reducing the abrasion during the tests [30].

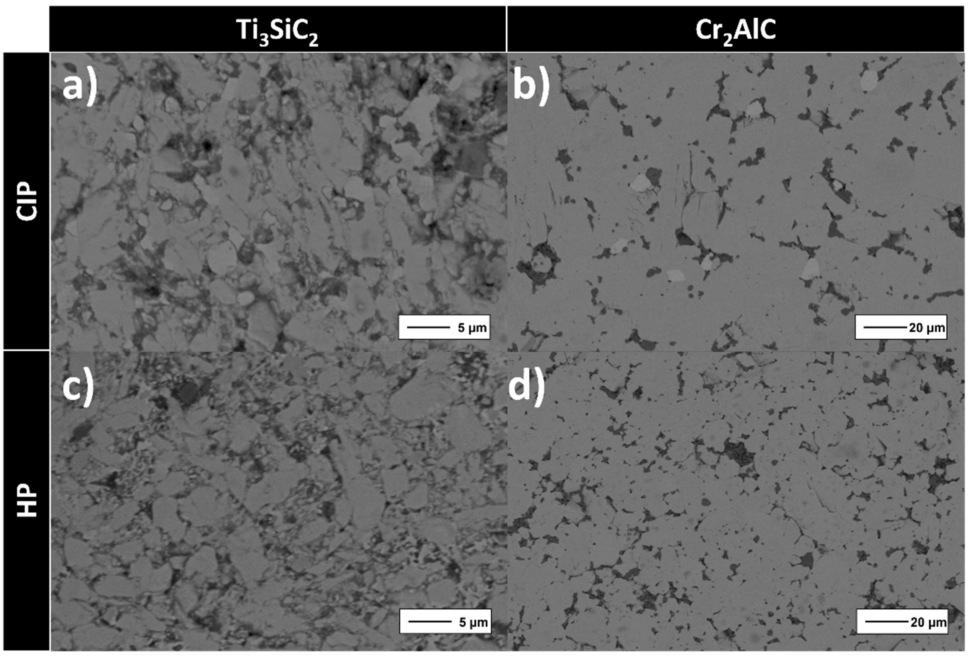

Figure 10. SEM micrographs of (**a**) cold isostatic pressed and sintered (CIP) Ti_3SiC_2; (**b**) cold isostatic pressed and sintered (CIP) Cr_2AlC; (**c**) hot-pressed (HP) Ti_3SiC_2 and (**d**) hot-pressed (HP) Cr_2AlC.

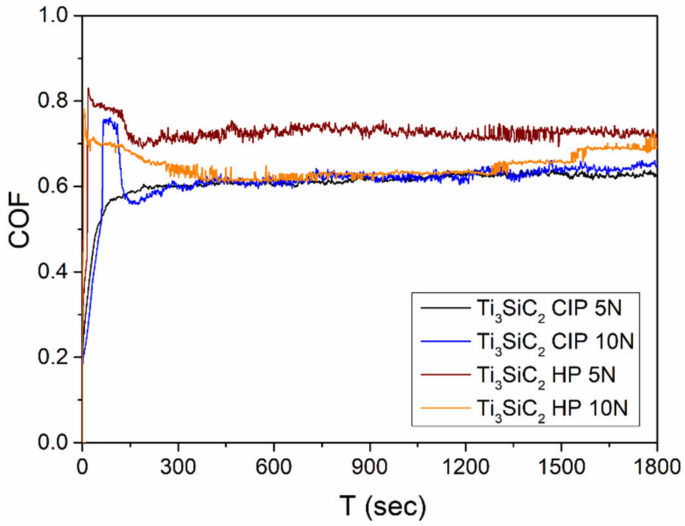

Figure 11. The coefficients of friction of the cold isostatic pressing and sintering (CIP) and hot-pressed (HP) samples during the reciprocating-sliding test with a load of 5 and 10 N of the Ti_3SiC_2 MAX phase.

On the other hand, hot-pressed Ti_3SiC_2 samples tested at 5 N and 10 N have higher final coefficients of friction, with a stabilization value at around 0.72 for both loads. In this case, a slightly higher coefficient during the test for the lowest load (5N) can be observed. Although this behavior is not expected, it could be due to the effect of the load in the delamination of the debris: in more aggressive conditions, it is easier to delaminate the material and generate a "lubricating" third body [12]. In Figure 12, it is possible to observe a higher final coefficient of friction for Cr_2AlC compared to those seen for Ti_3SiC_2. A possible explanation of this effect is the difficulty to produce wear in materials with a higher hardness (Ti_3SiC_2 = 4 GPa [22] and Cr_2AlC = 5.5 GPa [23]). The higher hardness of the Cr_2AlC MAX phase makes the wear debris more difficult to delaminate, thus reducing the self-lubricating effect and increasing the coefficient of friction. This double effect generated by the materials' hardness can also explain the difference between the CIP and

HP samples. HP samples have lower coefficients of friction and behave better than the CIP samples. It is important to note that hot pressing is a fast consolidation technique and the grain growth in this process is lower than for the CIP sample. This lower grain growth enhances the wear resistance of the HP samples [11]. In addition, as for the Ti_3SiC_2 hot-pressed samples, it is possible to see a lower COF for the Cr_2AlC HP 10 N than for the 5 N; this could be the effect of quicker delamination and faster oxidation of the debris [30], improving the wear resistance on the sample. When having more aggressive conditions set in the test, the higher load applied proves beneficial for the delamination of the debris, improving the self-lubricating effect of the MAX phases during wear.

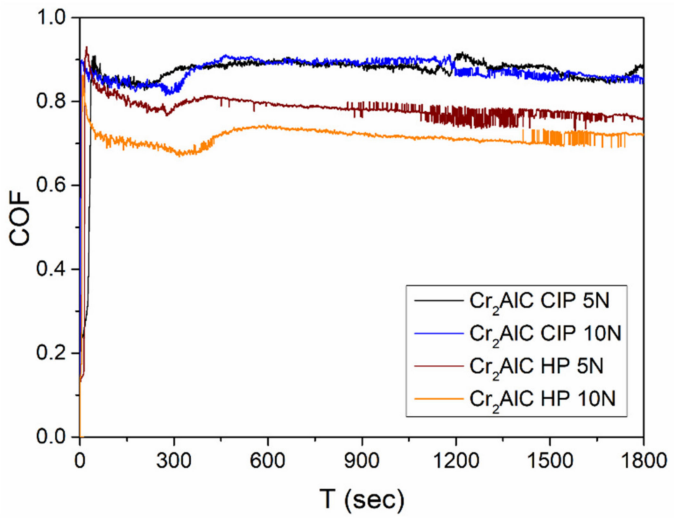

Figure 12. The coefficients of friction of the cold isostatic pressing and sintering (CIP) and hot-pressed (HP) samples during the reciprocating-sliding test with a load of 5 and 10 N of the Cr_2AlC MAX phase.

To better analyze the influence of the processing routes applied to obtain consolidated MAX phase samples, the wear rate was calculated. Figure 13 shows a representation of the 2D profiles of the wear tracks for different samples and loading conditions. In Figure 13a, the tracks of the cold isostatic and hot-pressed samples applying a load of 5N can be observed. From the track profiles, it can be noted that there is a better wear behavior for the Ti_3SiC_2 CIP sample that exhibits the smallest depth and width of the track. This effect is directly related to the porosity of the samples; with higher porosity, a higher amount of material is lost during the wear test. Thus, the cold isostatic pressed samples, which have lower porosity, have a smaller wear track profile compared to the hot-pressed samples that have higher porosity. This effect is also noticeable with the Cr_2AlC: both CIP and HP samples have similar porosity and similar wear track profiles. When comparing isostatic pressed samples, it is possible to observe a better wear behavior for MAX phase Ti_3SiC_2 compared to Cr_2AlC. This could be due to the differences between the self-lubricating effects of these MAX phase powders. As has been previously established, Ti_3SiC_2 has an intrinsic self-lubricating behavior [31] and Cr_2AlC has a strong dependence on the oxidation of the debris to generate this lubricating effect [30]. Furthermore, in terms of the debris formation, the difficulty of delaminating the torn material to produce this lubricating effect is also affected by the presence of secondary phases, which help to pin the MAX phase grains, delaying debris generation [31]. As can be seen in Figure 13a, this pinning effect is more noticeable for denser samples. As the porosity increases (hot-pressed Ti_3SiC_2), this pinning effect is no longer predominant and the debris generated could contain more secondary phases, creating more torn debris material with higher hardness and resulting in worse wear behavior. At higher loads (Figure 13b), as expected, the wear tracks are wider and deeper than those observed at 5 N. With these more aggressive conditions, we are able to observe a similar behavior for both MAX phases, no matter the processing route. The similarity of the CIP and HP 2D profiles for both MAX phases was not expected, since the

grain growth enhanced by the CIP sintering process should have had a negative effect on the wear behavior of the samples [11]. This effect is better understood with the wear rate calculation of the worn surfaces.

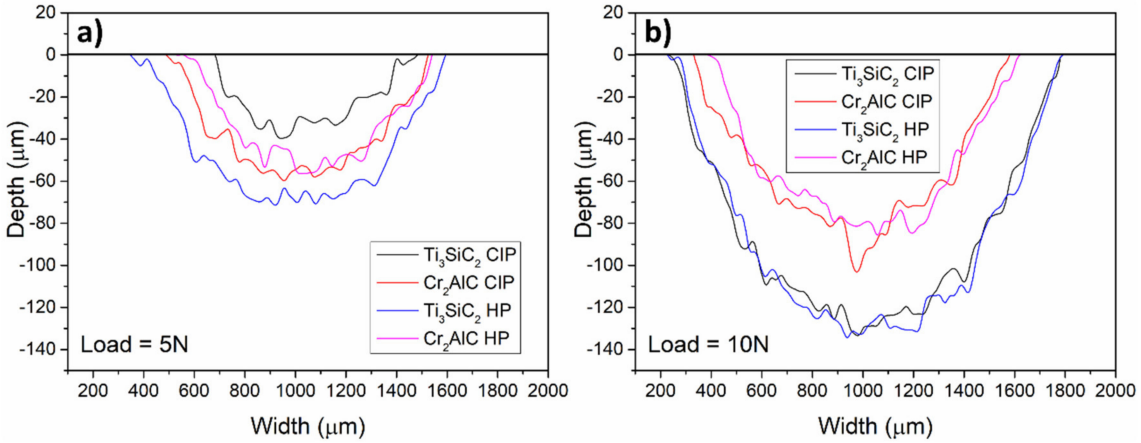

Figure 13. The 2D profiles at the center of the wear track of cold isostatic pressed and sintered (CIP) and hot-pressed (HP) Ti_3SiC_2 and Cr_2AlC applying (**a**) 5 N and (**b**) 10 N.

Although 2D profiles give a first approximation of the wear resistance of the materials, it is only a qualitative approach, and wear behavior should be studied by the wear rate, taking the complete track into consideration. The mean values of the profiles along the track and are shown in Table 5. In addition, the wear rates calculated following Equations (2)–(4) are shown in Figure 14.

Table 5. The wear track mean values extracted from the 2D profiles and the wear rate calculations for the Ti_3SiC_2 and Cr_2AlC MAX phases processed by CIP and HP.

MAX Phase	Process	Load (N)	Width (μm)	Depth (μm)	Area (mm^2)
Ti_3SiC_2	CIP	5	859.23	34.59	1.60×10^{-2}
		10	1610.72	133.59	1.46×10^{-1}
	HP	5	1006.23	55.76	3.86×10^{-2}
		10	1197.43	93.39	6.21×10^{-2}
Cr_2AlC	CIP	5	1212.16	77.10	5.54×10^{-2}
		10	1504.15	113.32	1.18×10^{-1}
	HP	5	977.78	48.10	2.87×10^{-2}
		10	1235.12	79.68	6.09×10^{-2}

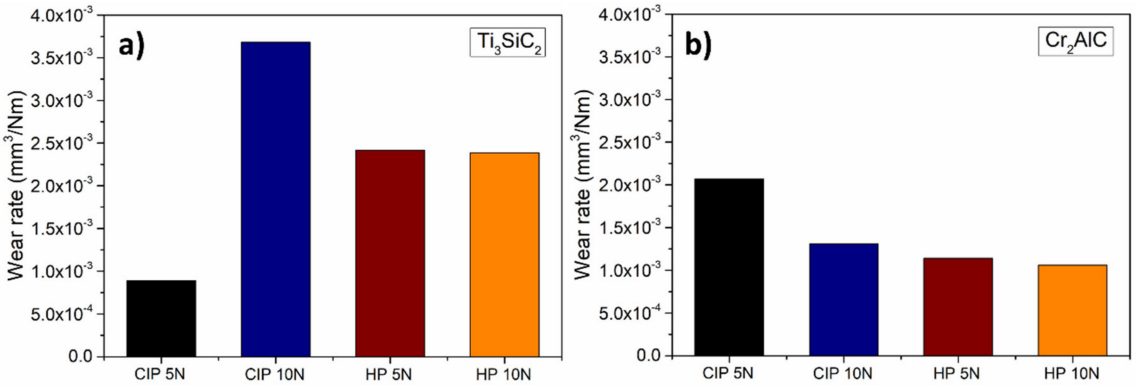

Figure 14. The wear rate calculations of samples processed by cold isostatic pressing and sintering (CIP) and hot pressing (HP) for (**a**) Ti_3SiC_2 and (**b**) Cr_2AlC.

It is possible to observe a high difference between the wear rates of CIP samples of Ti_3SiC_2 at different test loads. The CIP samples have the lowest porosity for this MAX phase, and under 5 N, exhibit the lowest wear rate of all the tested samples (8.91×10^{-4} mm^3/Nm). At higher loads, this wear rate increases greatly, reaching the highest value of all tested samples (3.68×10^{-3} mm^3/Nm). It appears that the larger grain size produced during the cold isostatic pressing and sintering has a detrimental effect on the wear behavior of these samples, as already seen in the hardness measurement shown in Table 4. At high loads, the CIP Ti_3SiC_2 sample dramatically decreases its wear properties. In this case, the amount of material removed during the test is not acting as lubricant debris, and as suspected from the COF measurements, the larger the grain size produced, the higher the difficulty in delaminating the debris. On the other hand, the hot-pressed Ti_3SiC_2 samples exhibit similar specific wear rates for 5 N and 10 N loads: 2.42×10^{-3} and 2.38×10^{-3} mm^3/Nm, respectively. This effect is directly related to the good wear behavior of the material and to an optimal consolidation of the samples, since a similar specific wear rate indicates a similar wear behavior under different conditions for the same sample.

The Cr_2AlC CIP sample exhibits an increase in the wear properties with an increase in the load, having specific wear rates of 2.07×10^{-3} mm^3/Nm at a load of 5 N and 1.31×10^{-3} mm^3/Nm at a load of 10 N. This could be due to the self-lubricating effect being enhanced in more severe loading conditions, which increases the delamination of the debris and improves the wear properties. In addition, the hot-pressed Cr_2AlC shows better wear properties and, similarly to HP Ti_3SiC_2, due to the lower grain size produced during the consolidation, indicates a good consolidation of the MAX phase samples and a good wear behavior of Cr_2AlC.

Complementary 3D profiles of the wear tracks are represented in Figure 15, where the color map representing the depth of each track depending on the load applied is shown.

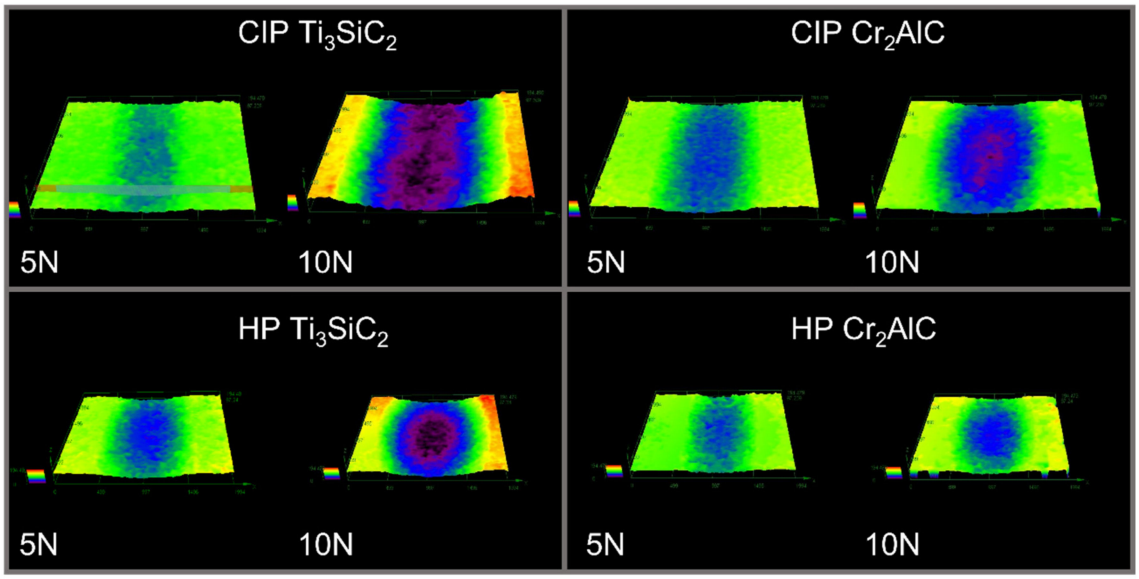

Figure 15. 3D profile images of the wear tracks for the Ti_3SiC_2 and Cr_2AlC MAX phases produced by cold isostatic pressing (CIP) and hot pressing (HP) at different wear test loads.

In order to study the wear mechanism produced during the tests, both secondary electron and back scattered detectors were analyzed to examine the nature of the wear. Wear test tracks for the 5 N load are shown in Figure 16 with an area analysis to study. If any amounts of oxygen and aluminum are found, that would suggest an adhesion of the aluminum ball used as counter material. An EDS analysis of the areas studied in Figure 16 is detailed in Table 6.

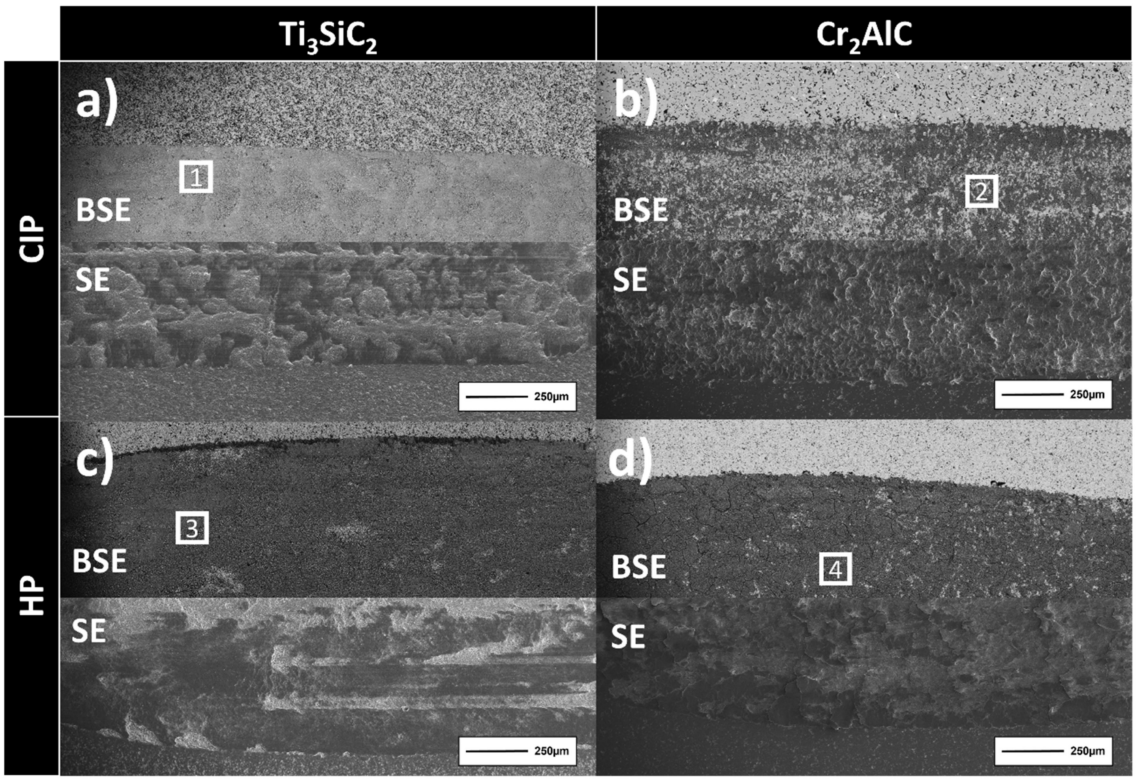

Figure 16. SEM secondary electron and back-scattered detectors micrographs of the reciprocating-sliding wear test with an applied load of 5 N for (**a**) cold isostatic pressed and sintered (CIP) Ti_3SiC_2; (**b**) cold isostatic pressed and sintered (CIP) Cr_2AlC; (**c**) hot-pressed (HP) Ti_3SiC_2 and (**d**) hot-pressed (HP) Cr_2AlC.

Table 6. An EDS area analysis of the wear tracks produced with a load of 5 N shown in the micrographs in Figure 16 for the cold isostatic pressing (CIP) and hot-pressed (HP) samples of the Ti_3SiC_2 and Cr_2AlC MAX phases.

Material/Process	Area	Ti (wt.%)	Cr (wt.%)	Si (wt.%)	Al (wt.%)	C (wt.%)	O (wt.%)
Ti_3SiC_2-CIP	1	36	-	12	10	26	16
Cr_2AlC-CIP	2	-	25	-	14	34	27
Ti_3SiC_2-HP	3	26	-	10	15	16	33
Cr_2AlC-HP	4	-	22	-	13	19	46

From the SEM micrographs, it is possible to observe a clear difference between MAX phases Ti_3SiC_2 and Cr_2AlC. The secondary electron detector shows horizontal lines corresponding to an abrasive mechanism in the Ti_3SiC_2 samples (Figure 16a,c) and some material accumulation in the form of stains corresponding to an adhesion of the counter material. Cr_2AlC (Figure 16b,d), on the other hand, exhibits a predominant adhesive mechanism, with no clear horizontal lines indicating abrasion. As reported elsewhere [32], it is possible to differentiate the wear behavior between both MAX phases. Ti_3SiC_2 behaves with a quasi-plastic deformation, with the formation of kink bands on the edges of the wear tracks (darker lines between the wear track and the substrate in Figure 16c). This is corroborated with the properties shown in Table 4, where the plastic work is higher for Ti_3SiC_2.

On the other hand, on Cr_2AlC, there is a formation of adhesive cracks within the wear track. Although in our work the adhesive behavior in worn Cr_2AlC is predominant, it is possible to observe those cracks in Figure 16b. This adhesive behavior, where the delamination of the MAX phase has been also previously reported [13] showing the adhesive nature of Cr_2AlC wear mechanism, reduces the coefficient of friction for samples with a higher

purity of Cr_2AlC. An EDS analysis in Table 6 confirms the adhesive mechanism through the detection of aluminum and oxygen in all the tracks and the predominant adhesive nature of the wear behavior for Cr_2AlC, exhibiting a higher oxygen content compared to that in the Ti_3SiC_2 produced by the same processing route. It is important to note that the presence of Al and O in Cr_2AlC could also be due to the formation and oxidation of debris, rather than from the Al_2O_3 counter material. Additionally, it is possible to observe a higher aluminum content for the Cr_2AlC samples tested at 5 N produced by hot pressing. These samples have a lower porosity, which should reduce the amount of debris created during the test and increase the adhesive wear mechanism in the samples.

The reciprocating-sliding wear tracks applying a load of 10 N are shown in Figure 17. It is possible to see the increase in the width of the wear tracks compared to those at a load of 5 N, as also seen in the 2D profiles. In this case, the horizontal lines indicating an abrasive wear observed previously are not seen at this higher load. This can be clearly seen in the Ti_3SiC_2 samples (Figure 17a,c), where big stains of adhered materials can be found in the BSE micrographs. The presence of more adherence zones at these higher loads is in accordance with the coefficient of friction and wear rates calculated, demonstrating a higher delamination of the MAX phases with the increase of the load to 10 N and improving the wear behavior of the material by increasing the self-lubricating effect during the test. Cr_2AlC (Figure 17b,d) exhibits this same behavior at 10 N. Under more aggressive conditions, it is possible to clearly observe in Figure 17d the cracking of the adhered debris formed during the test. As seen in the 5 N tests, the HP samples show a higher amount of adhered materials on the wear tracks when compared to the CIP samples; this can be attributed to the smaller grain size of the processed samples, which improves the delamination of the MAX phases. From the EDS analysis in Table 7, it is possible to demonstrate the predominant adhesive nature of the wear mechanism, mostly for the MAX phase Cr_2AlC with an increase in the oxygen found in the areas analyzed.

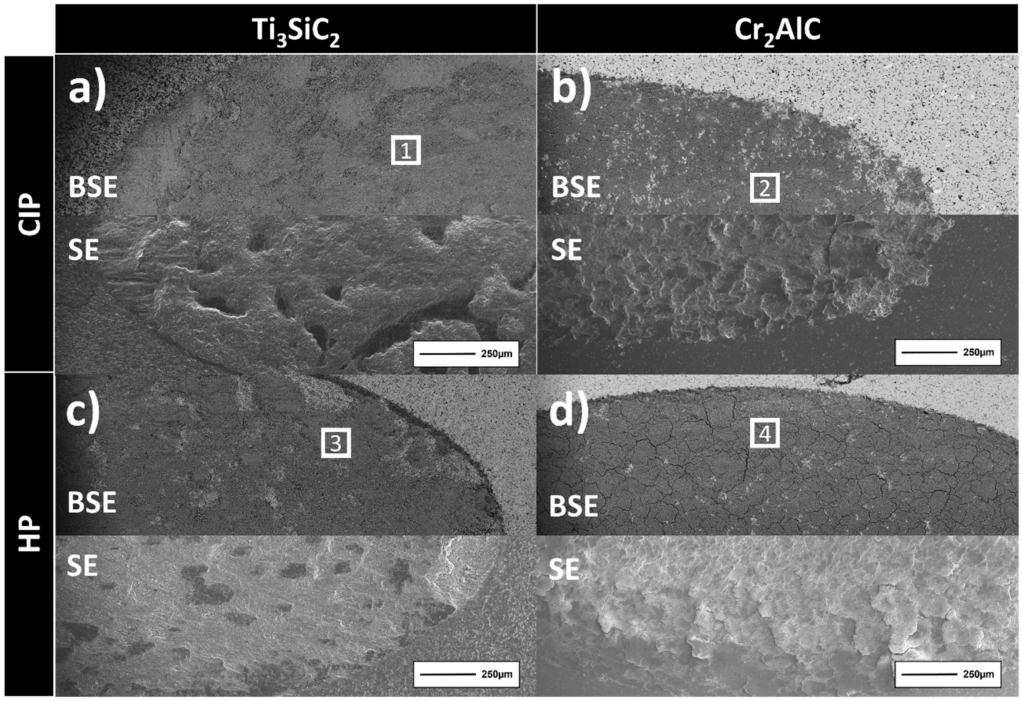

Figure 17. SEM secondary electron and back-scattered detectors micrographs of the reciprocating-sliding wear test with an applied load of 10 N for (**a**) cold isostatic pressed and sintered (CIP) Ti_3SiC_2; (**b**) cold isostatic pressed and sintered (CIP) Cr_2AlC; (**c**) hot-pressed (HP) Ti_3SiC_2 and (**d**) hot-pressed (HP) Cr_2AlC.

Table 7. An EDS area analysis of the wear tracks produced with a load of 10 N shown in the micrographs in Figure 17 for cold isostatic pressing (CIP) and hot-pressed (HP) samples of the Ti_3SiC_2 and Cr_2AlC MAX phases.

Material/Process	Area	Ti (wt.%)	Cr (wt.%)	Si (wt.%)	Al (wt.%)	C (wt.%)	O (wt.%)
Ti_3SiC_2-CIP	1	36	-	13	8	23	20
Cr_2AlC-CIP	2	-	17	-	11	20	52
Ti_3SiC_2-HP	3	30	-	12	15	19	24
Cr_2AlC-HP	4	-	18	-	11	21	50

4. Conclusions

The consolidation of self-synthesized Ti_3SiC_2 and Cr_2AlC was studied by three different processing techniques: uniaxial pressing and sintering, cold isostatic pressing and sintering and hot pressing. Each processing route has an effect on the final density of the samples and on the mechanical properties and wear behavior of the MAX phases. In terms of sinterability, hot pressing was the best processing technique for Cr_2AlC and cold isostatic pressing was the best processing technique for Ti_3SiC_2 due to the decomposition of the MAX phase during the inductive hot pressing of the powders, which lost most of their purity in the case of Ti_3SiC_2. An elastic modulus showed a close dependence on the porosity and the grain size of the sample. The CIP and sintered Ti_3SiC_2 samples exhibited the best properties, due to the reduction of porosity through the consolidation process. In the case of Cr_2AlC, an elastic modulus showed similar values for the HP samples compared to those previously reported. The compressive strength properties of the Ti_3SiC_2 and Cr_2AlC processed by CIP and HP were unaffected by the porosity and grain size and showed no hysteresis during the cyclic tests, with a similar behavior for the different processing routes.

The wear behavior of the MAX phases processed by CIP and HP was determined by comparing the different consolidation processes (CIP and HP) and varying the loads applied during the tests (5 and 10 N). For both MAX phases, wear behavior seems to have a dependence on the porosity of the samples. The CIP Ti_3SiC_2 exhibits the best wear properties at 5 N, which drastically decrease when increasing the load. However, in the case of hot-pressed samples, the wear behavior is similar for both applied loads. This effect is a combination of the grain size produced during the consolidation route and the self-lubricating effect of the MAX phases' debris generated during the tests. Cr_2AlC exhibits the same behavior for both consolidation routes, with a reduction on the wear rate when increasing the load; this reduction is higher for the CIP samples. This reduction is related to the ease of delaminating the debris by applying higher loads, which creates a self-lubricant effect during the wear test. Although both MAX phases revealed a self-lubricant effect, demonstrating the good wear properties of these materials, the wear mechanism of both MAX phases can be differentiated by a quasi-plastic deformation with a combination of abrasive and adhesive wear and a predominant adhesive wear mechanism for Cr_2AlC.

Author Contributions: E.T.: Writing—original draft, Conceptualization, Methodology, Investigation and Formal analysis. E.N.: Review and editing, Conceptualization, Methodology, Investigation and Formal analysis. M.K.: Review and editing, Conceptualization, Methodology, Investigation and Formal analysis. A.J.-M.: Review and editing, Conceptualization, Methodology, Investigation, Formal analysis and Resources. S.A.T.: Review and editing, Conceptualization, Methodology, Investigation, Formal analysis and Resources. All authors have read and agreed to the published version of the manuscript.

Funding: The authors would like to thank the funding provided for this research by the Regional Government of Madrid (Dra. Gral. Universidades e Investigación) through the project P2018/NMT4411 (ADITIMAT-CM), and the Spanish Government through the projects PID2019-106631GB-C43 and RTC2019-007049-4.

Institutional Review Board Statement: Not applicable.

Conflicts of Interest: The authors declare that they have no known competing financial interests or personal relationships that could have appeared to influence the work reported in this paper.

References

1. Hoffman, E.N.; Vinson, D.W.; Sindelar, R.L.; Tallman, D.J.; Kohse, G.; Barsoum, M.W. MAX phase carbides and nitrides: Properties for future nuclear power plant in-core applications and neutron transmutation analysis. *Nucl. Eng. Des.* **2012**, *244*, 17–24. [CrossRef]
2. Song, G.; Wang, Y.; Zhou, Y. *MAX Phases and Ultra-High Temperature Ceramics for Extreme Environments*; IGI Global: Hershey, PA, USA, 2013; ISBN 9781466640665.
3. Barsoum, M.W.; Radovic, M. Elastic and Mechanical Properties of the MAX Phases. *Annu. Rev. Mater. Res.* **2011**, *41*, 195–227. [CrossRef]
4. Barsoum, M.W. The Mn+1AXn Phases: A New Class of Solids. *Prog. Solid State Chem.* **2000**, *28*, 201–281. [CrossRef]
5. Barsoum, M. *MAX Phases: Properties of Machinable Ternary Carbides and Nitrides*; John Wiley & Sons: Hoboken, NJ, USA, 2013.
6. Jeitschko, W.; Nowotny, H. Die Kristallstruktur von Ti3SiC2: Ein neuer Komplexcarbid-Typ. *Mon. Für Chem.–Chem. Mon.* **1967**, *98*, 329–337. [CrossRef]
7. Tsipas, S.A.; Tabares, E.; Weissgaerber, T.; Hutsch, T.; Sket, F.; Velasco, B. Thermophysical properties of porous Ti2AlC and Ti3SiC2 produced by powder metallurgy. *J. Alloy. Compd.* **2021**, *857*, 158145. [CrossRef]
8. Velasco, B.; Gordo, E.; Hu, L.; Radovic, M.; Tsipas, S.A. Influence of porosity on elastic properties of Ti2AlC and Ti3SiC2 MAX phase foams. *J. Alloy. Compd.* **2018**, *764*, 24–35. [CrossRef]
9. Gonzalez-Julian, J.; Go, T.; Mack, D.E.; Vaßen, R. Thermal cycling testing of TBCs on Cr2AlC MAX phase substrates. *Surf. Coat. Technol.* **2018**, *340*, 17–24. [CrossRef]
10. Qarra, H.H.; Knowles, K.M.; Vickers, M.E.; Akhmadaliev, S.; Lambrinou, K. Heavy ion irradiation damage in Zr2AlC MAX phase. *J. Nucl. Mater.* **2019**, *523*, 1–9. [CrossRef]
11. El-Raghy, T.; Blau, P.; Barsoum, M.W. Effect of grain size on friction and wear behavior of Ti3SiC2. *Wear* **2000**, *238*, 125–130. [CrossRef]
12. Magnus, C.; Cooper, D.; Sharp, J.; Rainforth, W.M. Microstructural evolution and wear mechanism of Ti3AlC2—Ti2AlC dual MAX phase composite consolidated by spark plasma sintering (SPS). *Wear* **2019**, *438–439*, 203013. [CrossRef]
13. Shamsipoor, A.; Farvizi, M.; Razavi, M.; Keyvani, A. Influences of processing parameters on the microstructure and wear performance of Cr2AlC MAX phase prepared by spark plasma sintering method. *J. Alloy. Compd.* **2020**, *815*, 152345. [CrossRef]
14. Yu, W.; Chen, D.; Tian, L.; Zhao, H.; Wang, X. Self-lubricate and anisotropic wear behavior of AZ91D magnesium alloy reinforced with ternary Ti2AlC MAX phases. *J. Mater. Sci. Technol.* **2019**, *35*, 275–284. [CrossRef]
15. Ureña, J.; Tabares, E.; Tsipas, S.; Jiménez-Morales, A.; Gordo, E. Dry sliding wear behaviour of β-type Ti-Nb and Ti-Mo surfaces designed by diffusion treatments for biomedical applications. *J. Mech. Behav. Biomed. Mater.* **2019**, *91*, 335–344. [CrossRef] [PubMed]
16. Doni, Z.; Alves, A.C.; Toptan, F.; Gomes, J.R.; Ramalho, A.; Buciumeanu, M.; Palaghian, L.; Silva, F.S. Dry sliding and tribocorrosion behaviour of hot pressed CoCrMo biomedical alloy as compared with the cast CoCrMo and Ti6Al4V alloys. *Mater. Des.* **2013**, *52*, 47–57. [CrossRef]
17. Córdoba, J.M.; Sayagués, M.J.; Alcalá, M.D.; Gotor, F.J. Synthesis of Ti3SiC2 powders: Reaction mechanism. *J. Am. Ceram. Soc.* **2007**, *90*, 825–830. [CrossRef]
18. Gonzalez-Julian, J.; Onrubia, S.; Bram, M.; Guillon, O. Effect of sintering method on the microstructure of pure Cr2AlC MAX phase ceramics. *J. Ceram. Soc. Jpn.* **2016**, *124*, 415–420. [CrossRef]
19. Liu, X.L.; Jiang, Y.; Zhang, H.B.; He, Y.H. Corrosion behavior of porous Ti3SiC2 in nitric acid and aqua regia. *Trans. Nonferrous Met. Soc. China* **2017**, *27*, 584–590. [CrossRef]
20. Tabares, E.; Jiménez-Morales, A.; Tsipas, S.A. Study of the synthesis of MAX phase Ti3SiC2 powders by pressureless sintering. *Bol. La Soc. Esp. Ceram. Y Vidr.* **2020**, *60*, 41–52. [CrossRef]
21. Andersson, J.O.; Helander, T.; Höglund, L.; Shi, P.F.; Sundman, B. Thermo-Calc and DICTRA, Computational tools for materials science. *Calphad* **2002**, *26*, 273–312. [CrossRef]
22. El Saeed, M.A.; Deorsola, F.A.; Rashad, R.M. Optimization of the Ti3SiC2 MAX phase synthesis. *Int. J. Refract. Met. Hard Mater.* **2012**, *35*, 127–131. [CrossRef]
23. Lin, Z.; Zhou, Y.; Li, M.; Wang, J. In-situ hot pressing/solid-liquid reaction synthesis of bulk Cr2AlC. *Z. Fuer Met. Res. Adv. Tech.* **2005**, *96*, 291–296. [CrossRef]
24. Chen, Y.; Wang, N.; Ola, O.; Xia, Y.; Zhu, Y. Porous ceramics: Light in weight but heavy in energy and environment technologies. *Mater. Sci. Eng. R Rep.* **2021**, *143*, 100589. [CrossRef]
25. Hedayat, N.; Du, Y.; Ilkhani, H. Review on fabrication techniques for porous electrodes of solid oxide fuel cells by sacrificial template methods. *Renew. Sustain. Energy Rev.* **2017**, *77*, 1221–1239. [CrossRef]
26. Chen, X.; Xia, X.L.; Yan, X.W.; Sun, C. Heat transfer analysis of a volumetric solar receiver with composite porous structure. *Energy Convers. Manag.* **2017**, *136*, 262–269. [CrossRef]
27. Hammel, E.C.; Ighodaro, O.L.R.; Okoli, O.I. Processing and properties of advanced porous ceramics: An application based review. *Ceram. Int.* **2014**, *40*, 15351–15370. [CrossRef]

28. Fraczkiewicz, M.; Zhou, A.G.; Barsoum, M.W. Mechanical damping in porous Ti3SiC2. *Acta Mater.* **2006**, *54*, 5261–5270. [CrossRef]
29. Sun, Z.M.; Murugaiah, A.; Zhen, T.; Zhou, A.; Barsoum, M.W. Microstructure and mechanical properties of porous Ti3SiC2. *Acta Mater.* **2005**, *53*, 4359–4366. [CrossRef]
30. Gupta, S.; Filimonov, D.; Palanisamy, T.; Barsoum, M.W. Tribological behavior of select MAX phases against Al2O3 at elevated temperatures. *Wear* **2008**, *265*, 560–565. [CrossRef]
31. Magnus, C.; Cooper, D.; Ma, L.; Rainforth, W.M. Microstructures and intrinsic lubricity of in situ Ti3SiC2–TiSi2–TiC MAX phase composite fabricated by reactive spark plasma sintering (SPS). *Wear* **2020**, *448*, 203169. [CrossRef]
32. Qu, L.; Bei, G.; Nijemeisland, M.; Cao, D.; van der Zwaag, S.; Sloof, W.G. Point contact abrasive wear behavior of MAX phase materials. *Ceram. Int.* **2020**, *46*, 1722–1729. [CrossRef]